

# LIDAR REMOTE SENSING DATA COLLECTION: Clarks Fork & Hot Springs Creek, Montana

December 8, 2009

Submitted to:

Daniel March  
PBS&J  
3810 Valley Commons Drive, Suite 4  
Bozeman, MT 59718

Submitted by:

Watershed Sciences  
257B SW Madison Ave.  
Corvallis, OR 97333

529 SW 3rd Ave. Suite 300  
Portland, Oregon 97204



# LIDAR REMOTE SENSING DATA COLLECTION: CLARKS FORK & HOT SPRINGS CREEK, MT

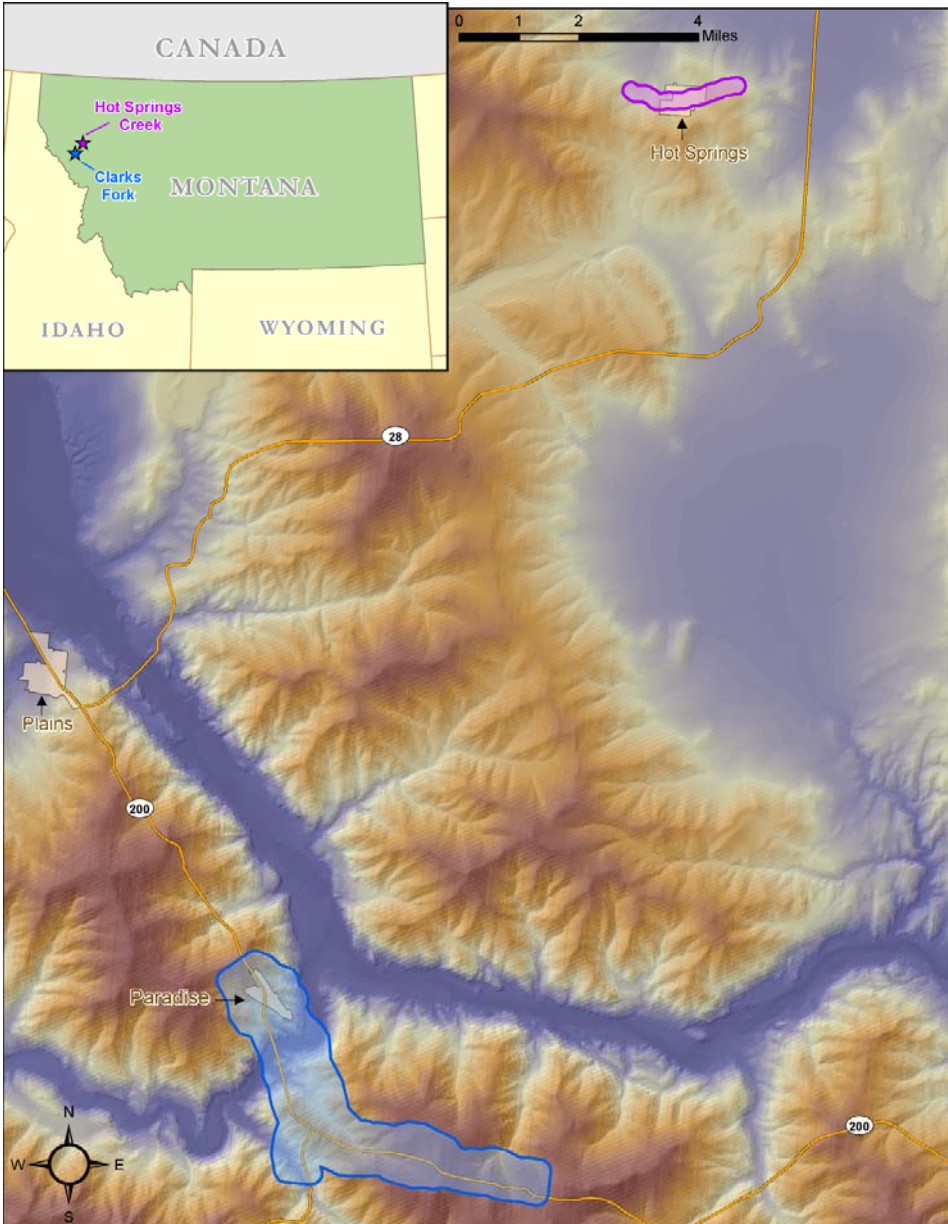
## TABLE OF CONTENTS

1. Overview .....	4
2. Acquisition .....	5
2.1 Airborne Survey - Instrumentation and Methods .....	5
2.2 Ground Survey - Instrumentation and Methods .....	6
2.2.1 Survey Control.....	6
2.2.2 RTK Survey.....	7
3. LiDAR Data Processing .....	10
3.1 Applications and Work Flow Overview .....	10
3.2 Aircraft Kinematic GPS and IMU Data.....	11
3.3 Laser Point Processing .....	11
4. LiDAR Accuracy Assessment .....	12
4.1 Laser Noise and Relative Accuracy.....	12
4.2 Absolute Accuracy .....	13
5. Study Area Results.....	14
5.1 Data Summary .....	14
5.2 Data Density/Resolution .....	14
5.3 Relative Accuracy Calibration Results.....	18
5.4 Absolute Accuracy .....	19
5.5 Accuracy per Land Cover .....	20
6. Bathymetric Survey .....	22
6.1 Overview .....	22
6.2 Bathymetric Survey - Instrumentation and Methods .....	24
6.3 Bathymetric Data Processing.....	24
6.4 Bathymetric Accuracy Assessment .....	25
7. Combined Elevation Model .....	26
7.1 Bathymetric Processing .....	27
7.2 Terrestrial LiDAR Extraction .....	27
7.3 Combined Elevation Model .....	27
8. Projection/Datum and Units.....	29
9. Deliverables .....	29
9. Selected Images .....	30
10. Glossary.....	35
11. Citations .....	36
Appendix A.....	37

# 1. Overview

Watershed Sciences, Inc. (WS) collected Light Detection and Ranging (LiDAR) data of Clarks Fork and Hot Springs Creek in northwestern Montana on September 21, 2009 and November 16, 2009 respectively. The total area of delivered LiDAR for Clarks Fork is 4943 acres and 373 acres for Hot Springs Creek (**Figure 1**). The requested area was expanded to include a 100 m buffer to ensure complete coverage and adequate point densities around survey area boundaries.

Figure 1. Clarks Fork and Hot Springs Creek Survey Areas.



## 2. Acquisition

### 2.1 Airborne Survey - Instrumentation and Methods

The LiDAR survey uses a Leica ALS50 Phase II laser system. For the Clarks Fork and Hot Springs Creek survey sites, the sensor scan angle was  $\pm 14^\circ$  from nadir<sup>1</sup> with a pulse rate designed to yield an average native density (number of pulses emitted by the laser system) of  $\geq 8$  points per square meter over terrestrial surfaces. All survey areas were surveyed with an opposing flight line side-lap of  $\geq 50\%$  ( $\geq 100\%$  overlap) to reduce laser shadowing and increase surface laser painting. The Leica ALS50 Phase II system allows up to four range measurements (returns) per pulse, and all discernable laser returns were processed for the output dataset. It is not uncommon for some types of surfaces (e.g. dense vegetation or water) to return fewer pulses than the laser originally emitted. These discrepancies between ‘native’ and ‘delivered’ density will vary depending on terrain, land cover and the prevalence of water bodies.



*The Cessna Caravan is a stable platform, ideal for flying slow and low for high density projects. The Leica ALS50 sensor head installed in the Caravan is shown on the left.*



To accurately solve for laser point position (geographic coordinates  $x, y, z$ ), the positional coordinates of the airborne sensor and the attitude of the aircraft were recorded continuously throughout the LiDAR data collection mission. Aircraft position was measured twice per second (2 Hz) by an onboard differential GPS unit. Aircraft attitude was measured 200 times per second (200 Hz) as pitch, roll and yaw (heading) from an onboard inertial measurement unit (IMU). To allow for post-processing correction and calibration, aircraft/sensor position and attitude data are indexed by GPS time.

---

<sup>1</sup> Nadir refers to the perpendicular vector to the ground directly below the aircraft. Nadir is commonly used to measure the angle from the vector and is referred to a “degrees from nadir”.

## 2.2 Ground Survey - Instrumentation and Methods

The following ground survey data were collected to enable the geo-spatial correction of the aircraft positional coordinate data collected throughout the flight, and to allow for quality assurance checks on final LiDAR data products.

### 2.2.1 Survey Control

Simultaneous with the airborne data collection mission, we conducted multiple static (1 Hz recording frequency) ground surveys over monuments with PLS certified coordinates (Table 1). Indexed by time, these GPS data are used to correct the continuous onboard measurements of aircraft position recorded throughout the mission. Multiple sessions were processed over the same monument to confirm antenna height measurements and reported position accuracy. After the airborne survey, these static GPS data were then processed using triangulation with Continuously Operating Reference Stations (CORS) stations, and checked against the Online Positioning User Service (OPUS<sup>2</sup>) to quantify daily variance. Controls were located within 13 nautical miles of the mission area(s).



---

<sup>2</sup> Online Positioning User Service (OPUS) is run by the National Geodetic Survey to process corrected monument positions.

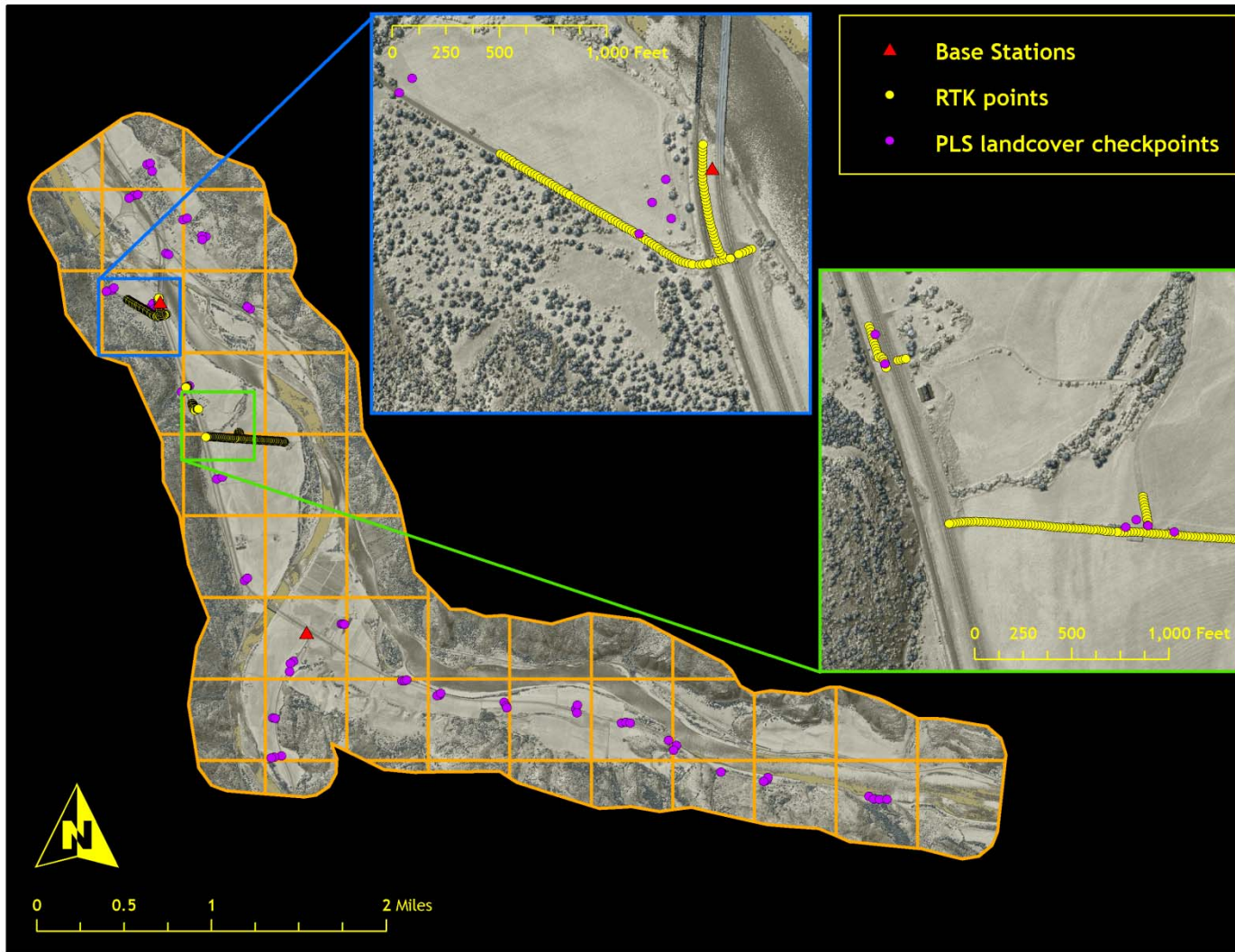
*Table 1. Base Station Survey Control coordinates for the Clarks Fork and Hot Springs Creek survey areas.*

Base Station ID	Datum: NAD83 (CORS91)		GRS80
	Latitude	Longitude	Ellipsoid Z (feet)
HSPWH1 (PCI)	47° 36' 46.898"	114° 39' 29.359"	2754.262
HSPWH2 (PCI)	47° 36' 35.155"	114° 40' 36.360"	2858.127
WGM1 (WGM)	47° 22' 51.114"	114° 47' 59.866"	2451.537
WGM2 (WGM)	47° 21' 15.730"	114° 46' 45.939"	2446.111

### 2.2.2 RTK Survey

To enable assessment of LiDAR data accuracy, ground truth points were collected using GPS based real-time kinematic (RTK) surveying. For an RTK survey, the ground crew uses a roving unit to receive radio-relayed corrected positional coordinates for all ground points from a GPS base station set up over a survey control monuments. The Clarks Fork monuments were certified by WGM Group (P.L.S Montana Registration No. 17477LS) and the Hot Springs monuments were certified by PCI (P.L.S Montana Registration No. 12252S). Instrumentation includes multiple Trimble DGPS units (R8). RTK surveying allows for precise location measurements with an error ( $\sigma$ ) of  $\leq 1.5$  cm (0.6 in). **Figures 2 & 3** below portray a distribution of RTK point locations used for the Clarks Fork and Hot Springs Creek survey areas.

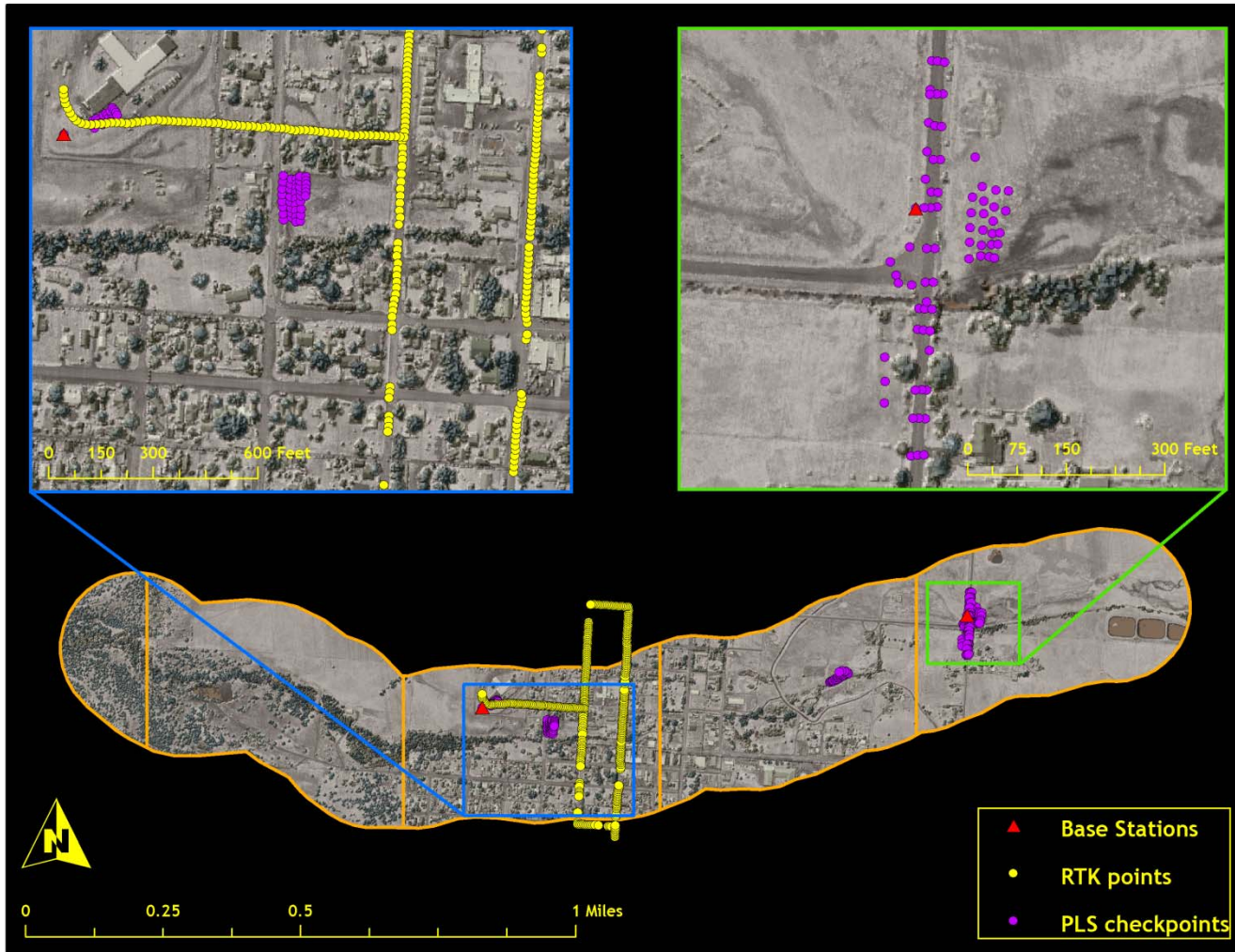
Figure 2. RTK, PLS land cover checkpoints, and control monument locations used for the Clarks Fork Creek Survey area.



LiDAR Data Acquisition and Processing: Clarks Fork & Hot Springs Creek, Montana

Prepared by Watershed Sciences, Inc.

Figure 3. RTK, PLS land cover checkpoints, and control monument locations used for the Hot Springs Survey area. Many RTK points lie outside the delivered Hot Spring boundary due to LiDAR coverage extending outside the AOI. These points are retained for reporting because of their use in calibration of the raw data.



LiDAR Data Acquisition and Processing: Clarks Fork & Hot Springs Creek, Montana

Prepared by Watershed Sciences, Inc.

## 3. LiDAR Data Processing

### 3.1 Applications and Work Flow Overview

1. Resolved kinematic corrections for aircraft position data using kinematic aircraft GPS and static ground GPS data.  
**Software:** Waypoint GPS v.8.10, Trimble Geomatics Office v.1.62
2. Developed a smoothed best estimate of trajectory (SBET) file that blends post-processed aircraft position with attitude data. Sensor head position and attitude were calculated throughout the survey. The SBET data were used extensively for laser point processing.  
**Software:** IPAS v.1.4
3. Calculated laser point position by associating SBET position to each laser point return time, scan angle, intensity, etc. Created raw laser point cloud data for the entire survey in \*.las (ASPRS v. 1.2) format.  
**Software:** ALS Post Processing Software v.2.69
4. Imported raw laser points into manageable blocks (less than 500 MB) to perform manual relative accuracy calibration and filter for pits/birds. Ground points were then classified for individual flight lines (to be used for relative accuracy testing and calibration).  
**Software:** TerraScan v.9.001
5. Using ground classified points per each flight line, the relative accuracy was tested. Automated line-to-line calibrations were then performed for system attitude parameters (pitch, roll, heading), mirror flex (scale) and GPS/IMU drift. Calibrations were performed on ground classified points from paired flight lines. Every flight line was used for relative accuracy calibration.  
**Software:** TerraMatch v.9.001
6. Position and attitude data were imported. Resulting data were classified as ground and non-ground points. Statistical absolute accuracy was assessed via direct comparisons of ground classified points to ground RTK survey data. Data were then converted to orthometric elevations (NAVD88) by applying a Geoid03 correction. Ground models were created as a triangulated surface and exported as ArcInfo ASCII grids at a 3 foot pixel resolution.  
**Software:** TerraScan v.9.001, ArcMap v. 9.3.1, TerraModeler v.9.001

## 3.2 Aircraft Kinematic GPS and IMU Data

LiDAR survey datasets were referenced to the 1 Hz static ground GPS data collected over pre-surveyed monuments with known coordinates. While surveying, the aircraft collected 2 Hz kinematic GPS data, and the onboard inertial measurement unit (IMU) collected 200 Hz aircraft attitude data. Waypoint GPS v.8.10 was used to process the kinematic corrections for the aircraft. The static and kinematic GPS data were then post-processed after the survey to obtain an accurate GPS solution and aircraft positions. IPAS v.1.4 was used to develop a trajectory file that includes corrected aircraft position and attitude information. The trajectory data for the entire flight survey session were incorporated into a final smoothed best estimated trajectory (SBET) file that contains accurate and continuous aircraft positions and attitudes.

## 3.3 Laser Point Processing

Laser point coordinates were computed using the IPAS and ALS Post Processor software suites based on independent data from the LiDAR system (pulse time, scan angle), and aircraft trajectory data (SBET). Laser point returns (first through fourth) were assigned an associated (x, y, z) coordinate along with unique intensity values (0-255). The data were output into large LAS v. 1.2 files; each point maintains the corresponding scan angle, return number (echo), intensity, and x, y, z (easting, northing, and elevation) information.

These initial laser point files were too large for subsequent processing. To facilitate laser point processing, bins (polygons) were created to divide the dataset into manageable sizes (< 500 MB). Flightlines and LiDAR data were then reviewed to ensure complete coverage of the survey area and positional accuracy of the laser points.

Laser point data were imported into processing bins in TerraScan, and manual calibration was performed to assess the system offsets for pitch, roll, heading and scale (mirror flex). Using a geometric relationship developed by Watershed Sciences, each of these offsets was resolved and corrected if necessary.

LiDAR points were then filtered for noise, pits (artificial low points) and birds (true birds as well as erroneously high points) by screening for absolute elevation limits, isolated points and height above ground. Each bin was then manually inspected for remaining pits and birds and spurious points were removed. In a bin containing approximately 7.5-9.0 million points, an average of 50-100 points are typically found to be artificially low or high. Common sources of non-terrestrial returns are clouds, birds, vapor, haze, decks, brush piles, etc.

Internal calibration was refined using TerraMatch. Points from overlapping lines were tested for internal consistency and final adjustments were made for system misalignments (i.e., pitch, roll, heading offsets and scale). Automated sensor attitude and scale corrections yielded 3-5 cm improvements in the relative accuracy. Once system misalignments were corrected, vertical GPS drift was then resolved and removed per flight line, yielding a slight improvement (<1 cm) in relative accuracy.

The TerraScan software suite is designed specifically for classifying near-ground points (Soininen, 2004). The processing sequence began by 'removing' all points that were not

---

LiDAR Data Acquisition and Processing: Clarks Fork & Hot Springs Creek, Montana

'near' the earth based on geometric constraints used to evaluate multi-return points. The resulting bare earth (ground) model was visually inspected and additional ground point modeling was performed in site-specific areas to improve ground detail. This manual editing of grounds often occurs in areas with known ground modeling deficiencies, such as: bedrock outcrops, cliffs, deeply incised stream banks, and dense vegetation. In some cases, automated ground point classification erroneously included known vegetation (i.e., understory, low/dense shrubs, etc.). These points were manually reclassified as non-grounds. Ground surface rasters were developed from triangulated irregular networks (TINs) of ground points.

## 4. LiDAR Accuracy Assessment

Our LiDAR quality assurance process uses the data from the real-time kinematic (RTK) ground survey conducted in the survey area. In this project, a total of **637 RTK GPS** measurements were collected on hard surfaces distributed among multiple flight swaths. To assess absolute accuracy, we compared the location coordinates of these known RTK ground survey points to those calculated for the closest laser points.

### 4.1 Laser Noise and Relative Accuracy

Laser point absolute accuracy is largely a function of laser noise and relative accuracy. To minimize these contributions to absolute error, we first performed a number of noise filtering and calibration procedures prior to evaluating absolute accuracy.

#### *Laser Noise*

For any given target, laser noise is the breadth of the data cloud per laser return (i.e., last, first, etc.). Lower intensity surfaces (roads, rooftops, still/calm water) experience higher laser noise. The laser noise range for this survey was approximately 0.02 meters.

#### *Relative Accuracy*

Relative accuracy refers to the internal consistency of the data set - the ability to place a laser point in the same location over multiple flight lines, GPS conditions, and aircraft attitudes. Affected by system attitude offsets, scale, and GPS/IMU drift, internal consistency is measured as the divergence between points from different flight lines within an overlapping area. Divergence is most apparent when flight lines are opposing. When the LiDAR system is well calibrated, the line-to-line divergence is low (<10 cm). See Appendix A for further information on sources of error and operational measures that can be taken to improve relative accuracy.

#### **Relative Accuracy Calibration Methodology**

1. **Manual System Calibration:** Calibration procedures for each mission require solving geometric relationships that relate measured swath-to-swath deviations to misalignments of system attitude parameters. Corrected scale, pitch, roll and heading offsets were calculated and applied to resolve misalignments. The raw divergence between lines was computed after the manual calibration was completed and reported for each survey area.
2. **Automated Attitude Calibration:** All data were tested and calibrated using TerraMatch automated sampling routines. Ground points were classified for each individual flight line and used for line-to-line testing. System misalignment offsets (pitch, roll and

heading) and scale were solved for each individual mission and applied to respective mission datasets. The data from each mission were then blended when imported together to form the entire area of interest.

3. Automated Z Calibration: Ground points per line were utilized to calculate the vertical divergence between lines caused by vertical GPS drift. Automated Z calibration was the final step employed for relative accuracy calibration.

## 4.2 Absolute Accuracy

The vertical accuracy of the LiDAR data is described as the mean and standard deviation ( $\sigma$ ) of divergence of LiDAR point coordinates from RTK ground survey point coordinates. To provide a sense of the model predictive power of the dataset, the root mean square error (RMSE) for vertical accuracy is also provided. These statistics assume the error distributions for x, y, and z are normally distributed, thus we also consider the skew and kurtosis of distributions when evaluating error statistics.

Statements of statistical accuracy apply to fixed terrestrial surfaces only and may not be applied to areas of dense vegetation or steep terrain. To calibrate laser accuracy for the LiDAR dataset, 637 RTK points were collected on fixed, hard-packed road surfaces within the survey area.

## 5. Study Area Results

Summary statistics for point resolution and accuracy (relative and absolute) of the LiDAR data collected in the Clarks Fork and Hot Springs Creek survey area are presented below in terms of central tendency, variation around the mean, and the spatial distribution of the data (for point resolution by bin).

### 5.1 Data Summary

Table 2. Resolution and Accuracy - Specifications and Achieved Values

	Targeted	Achieved
Resolution:	$\geq 8$ points/m <sup>2</sup>	0.70 points/ft <sup>2</sup> (7.53 points/m <sup>2</sup> )
*Vertical Accuracy (1 $\sigma$ ):	<15 cm	0.095 ft (2.90 cm)

\* Based on 637 hard-surface control points

### 5.2 Data Density/Resolution

The average data density across the survey area is 7.53 points per square meter (.70 points per square foot)(Table 2). Some types of surfaces (i.e., dense vegetation, breaks in terrain, steep slopes, water) may return fewer pulses (delivered density) than the laser originally emitted (native density). Because both the Clarks Fork and Hot Springs Creek survey focused on the river and valley bottom, some bins had a high proportion of water and thus a slightly lower delivered data density. Ground classifications were derived from automated ground surface modeling and manual, supervised classifications where it was determined that the automated model had failed. Ground return densities will be lower in areas of dense vegetation, water, or buildings. The ground-classified point map in Figure 6 & 7 identifies these areas of lower ground return densities.

Data Resolution for the Clarks Fork and Hot Springs Creek survey area:

- Combined Average Point (First Return) Density = 0.70 points/ft<sup>2</sup> (7.53 points/m<sup>2</sup>)
- Combined Average Ground Point Density = 0.17 points/ft<sup>2</sup> (1.83 points/m<sup>2</sup>)

Figure 4. Density distribution for first return laser points

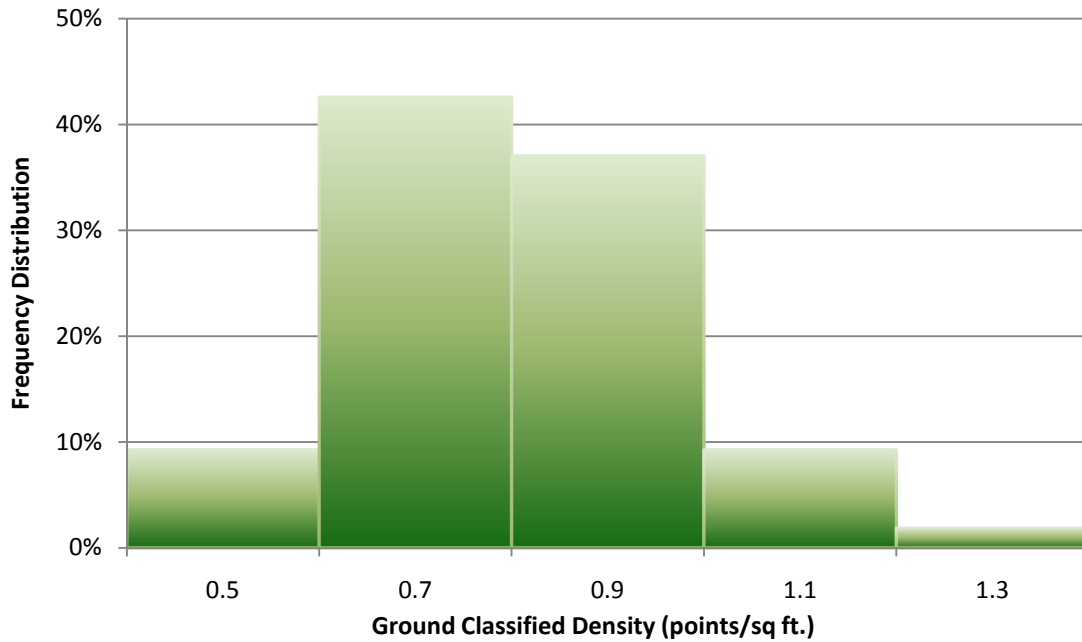


Figure 5. Density distribution for ground-classified laser points.

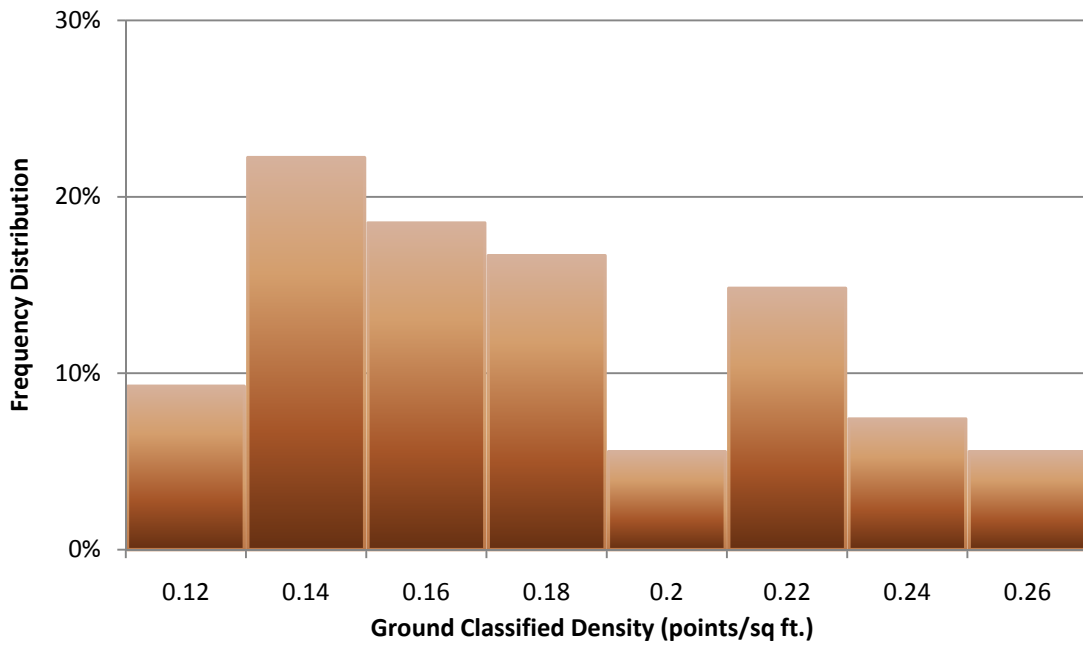
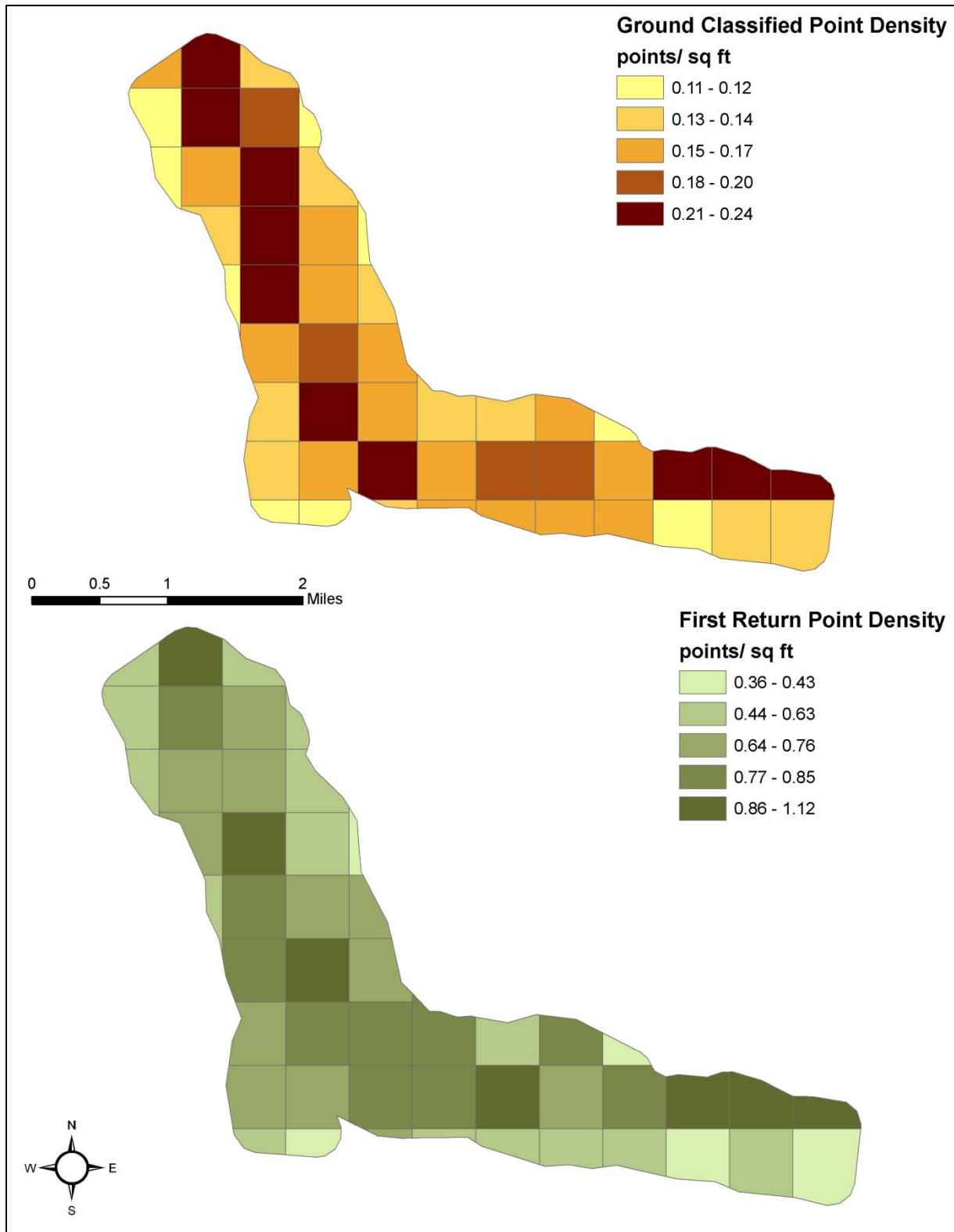


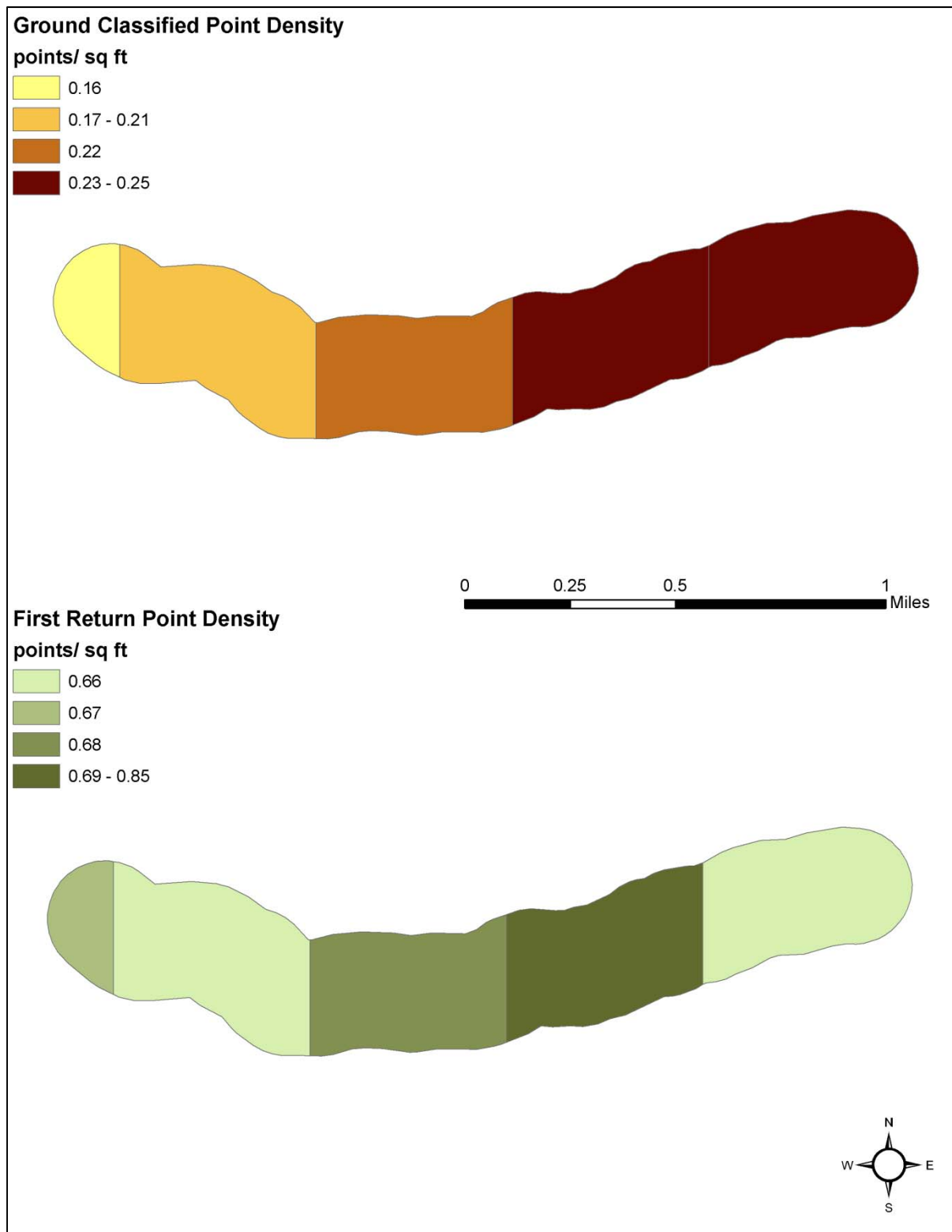
Figure 6. Clarks Fork Density distribution map for first return and ground classified points



LiDAR Data Acquisition and Processing: Clarks Fork & Hot Springs Creek, Montana

Prepared by Watershed Sciences, Inc.

Figure 7. Hot Springs Density distribution map for first return and ground classified points

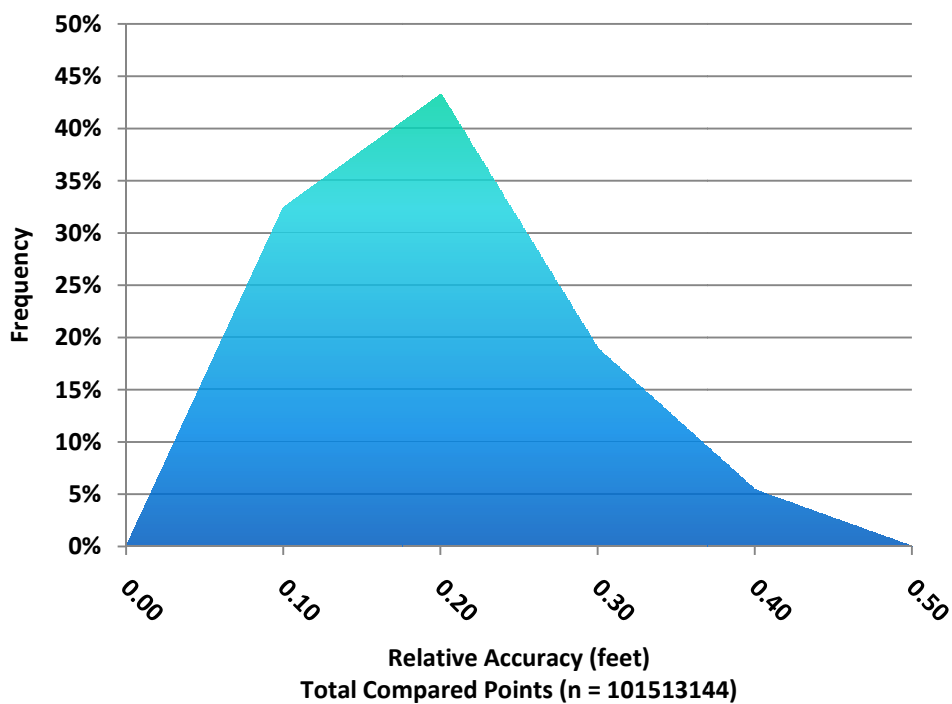


### 5.3 Relative Accuracy Calibration Results

Relative accuracies for the Clarks Fork and Hot Springs Creek survey area:

- Project Average = 0.158 ft (0.048m)
- Median Relative Accuracy = 0.153ft (0.047m)
- 1 $\sigma$  Relative Accuracy = 0.176ft (0.054m)
- 2 $\sigma$  Relative Accuracy = 0.297ft (0.091m)

Figure 8. Distribution of relative accuracies per flight line, non slope-adjusted



## 5.4 Absolute Accuracy

Absolute accuracies for the Clarks Fork and Hot Springs Creek survey areas

Table 3. Absolute Accuracy - Deviation between laser points and RTK hard surface survey points

RTK Survey Sample Size (n): 637	
Root Mean Square Error (RMSE) = 0.095 ft (0.029m)	Minimum $\Delta z$ = -0.400ft (-.122m)
Standard Deviations 1 sigma ( $\sigma$ ): 0.089ft (0.027m)      2 sigma ( $\sigma$ ): 0.177ft (0.054m)	Maximum $\Delta z$ = 1.141 ft (0.106m)
	Average $\Delta z$ = -0.005ft (-0.002m)

Figure 9. Absolute Accuracy - Histogram Statistics, based on 637 hard surface points

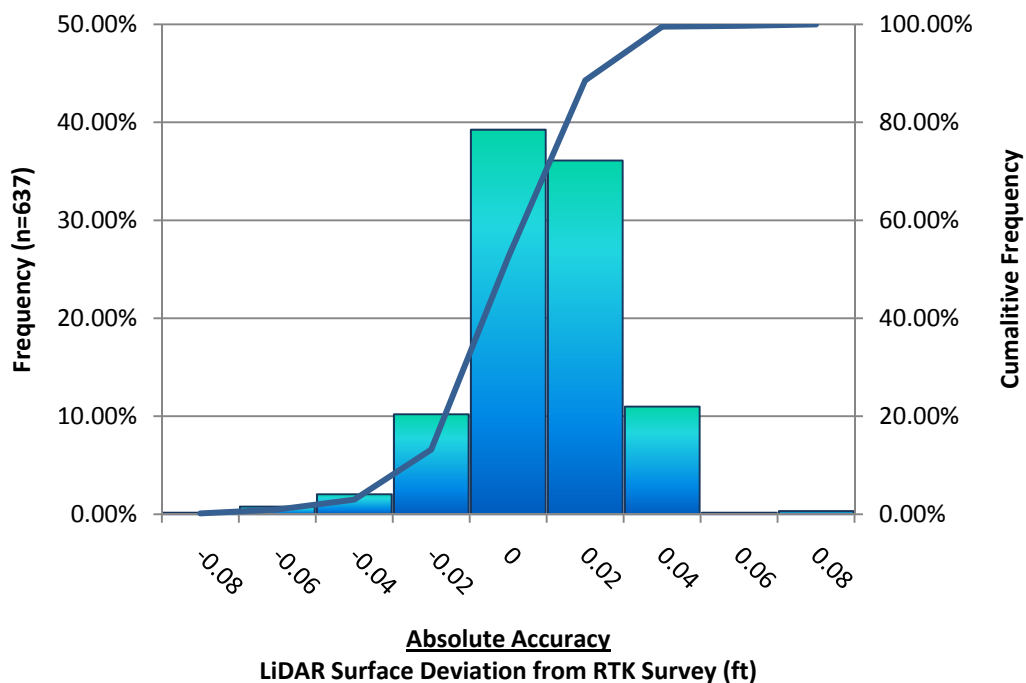
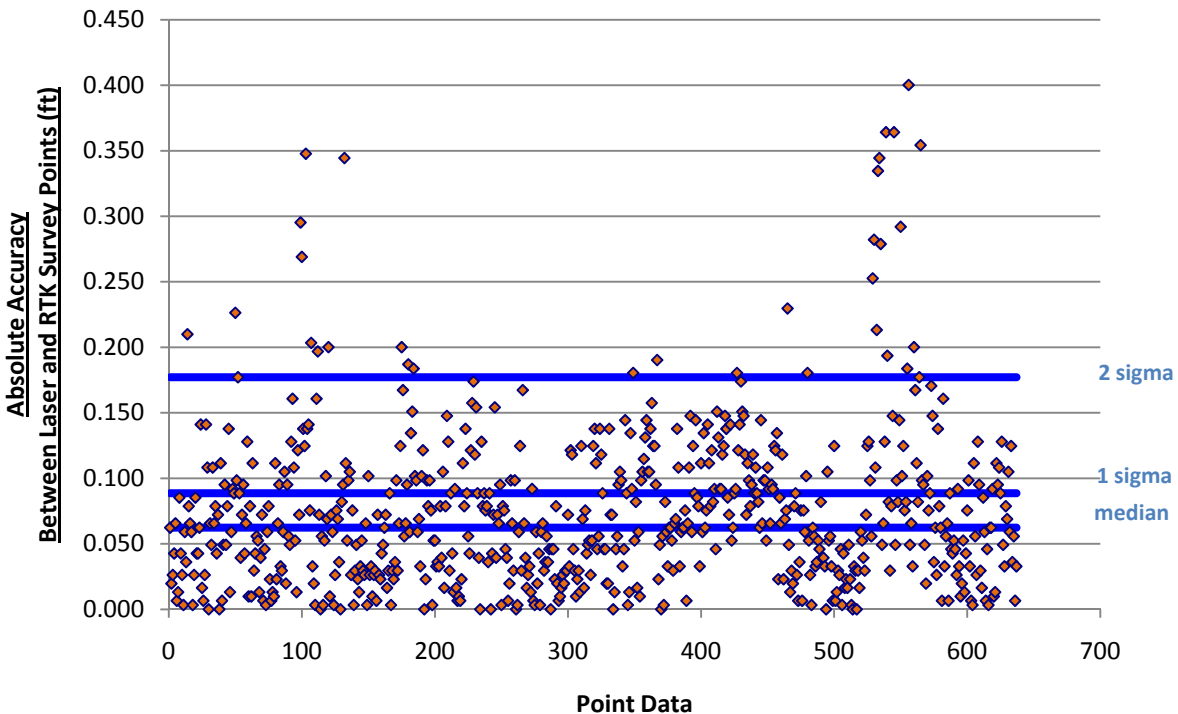


Figure 10. Absolute Accuracy - Absolute Deviation, based on hard surface points



## 5.5 Accuracy per Land Cover

In addition to the hard surface RTK data collection, points were also collected independently on different land cover types. Individual accuracies were calculated for each land-cover type to assess confidence in the LiDAR derived ground models across land-cover classes. Accuracy statistics for each land cover class are reported in Table 4 and 5.

The land cover classes for Clarks Fork study area include:

Bare Earth and low grass: Open, barely vegetated surfaces, (e.g. plowed fields and lawns).

High Grasses: Generally incorporates weeds and crops (e.g. hay fields, corn fields and wheat fields).

Brush lands: Shrubs and low trees (e.g. chaparrals and mesquite).

Table 4. Summary of absolute accuracy statistics for each land cover type at Hot Springs Creek

Land cover	Sample size (n)	Mean Dz : feet	1 sigma ( $\sigma$ ): feet	1.96 sigma ( $\sigma$ ): feet	RMSE: feet
Bare Earth and low grass	29	0.06	0.103	0.229	0.116
High Grasses	24	0.288	0.285	0.456	0.379
Brush Lands	23	0.352	0.417	1.176	0.577

The land cover classes for Hot Springs Creek study area include:

Asphalt: Bare non-vegetated surfaces (e.g. roads, sidewalks, and parking lots).

Bare Earth: Open, barely vegetated surfaces, (e.g. plowed fields, lawns, and golf course).

Gravel: Bare rocky surfaces (e.g. gravel roads).

Grasses: Surfaces with low grasses (e.g. lawns)

Tall Vegetation: Generally incorporates weeds and crops (e.g. hay fields, corn fields, and wheat fields).

Table 5. Summary of absolute accuracy statistics for each land cover type at Hot Springs Creek

Land cover	Sample size (n)	Mean Dz : feet	1 sigma ( $\sigma$ ): feet	1.96 sigma ( $\sigma$ ): feet	RMSE: feet
Asphalt	42	-0.07	0.07	0.16	0.09
Bare Earth	40	0.02	0.07	0.13	0.08
Gravel	23	-0.05	0.07	0.11	0.07
Grasses	26	0.14	0.17	0.27	0.16
Tall Vegetation	28	0.45	0.46	0.7	0.47

This analysis shows that the vertical accuracy of the interpolated ground surface meets or exceeds vertical accuracy specifications for bare earth cover type.

## 6. Bathymetric Survey

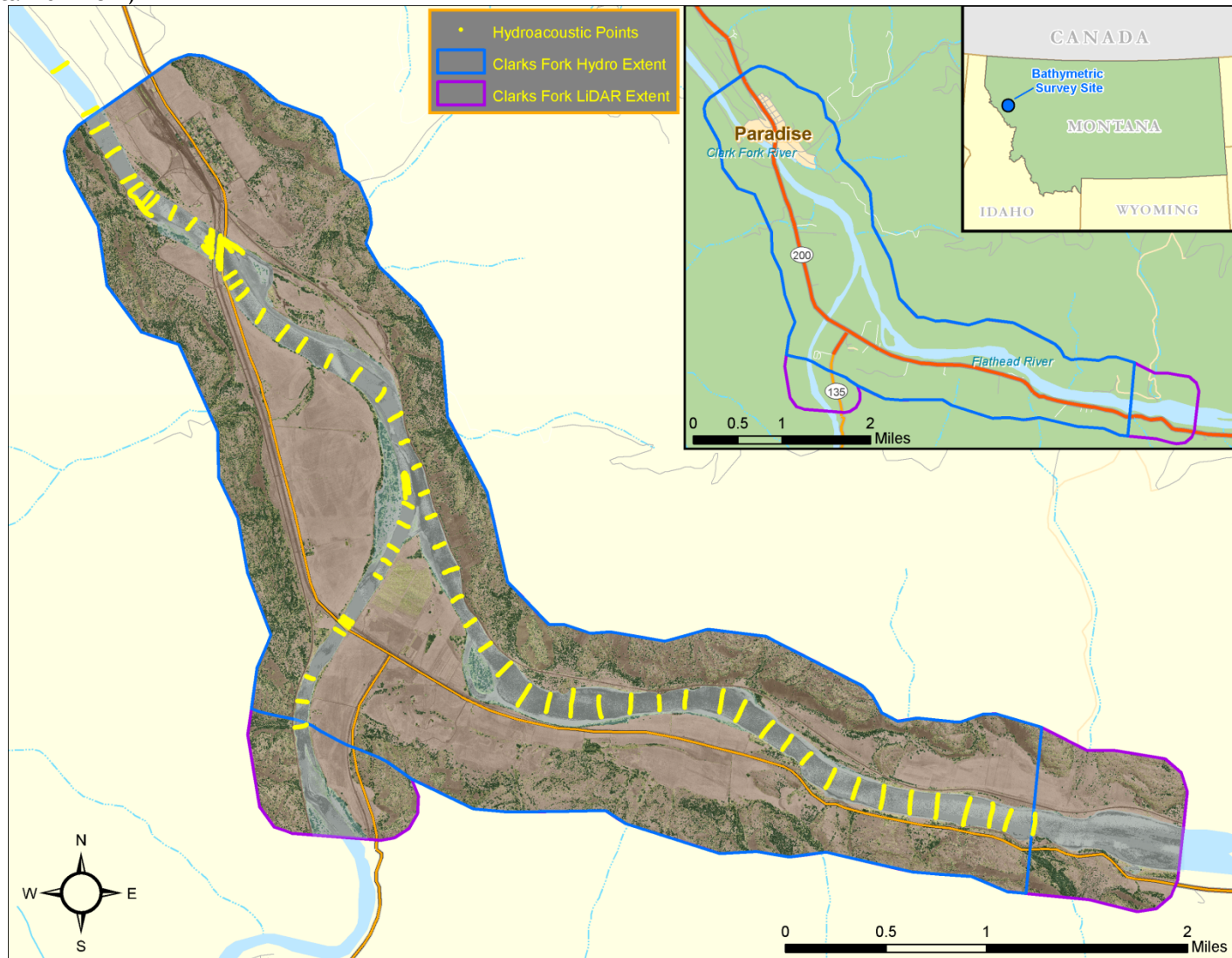
### 6.1 Overview

A bathymetric survey was conducted over a portion of the Clarks Fork LiDAR survey area using hydro-acoustic technology. Since the airborne LiDAR does not penetrate water surface, hydro-acoustic data were collected to provide a continuous terrain surface model to support hydraulic and engineering analysis in the study reaches. The bathymetry data were collected on September 19<sup>th</sup> and 20<sup>th</sup>, 2009 by MaxDepth Aquatics, Bend, OR. This data set provides a spatially continuous compliment to the high resolution LiDAR data. The two data sets were integrated by Watershed Sciences to produce a seamless combined elevation model. This section provides a detailed overview of the collection and processing of the hydro-acoustic data.

The bathymetric data were collected on 67 pre-mapped cross sections that were spaced between 20 and 300 meters apart depending on the study reach. Additional bathymetric points were taken longitudinally in side and off-channel areas as access permitted. Figure 11 illustrates the distribution of bathymetric data collected.

The bathymetric data were collected on a subset of the total LiDAR area.

Figure 11. Distribution of hydroacoustic data and extent of LiDAR / hydroacoustic integration (Highest-hit LiDAR over Intensities with street and town data from ESRI)

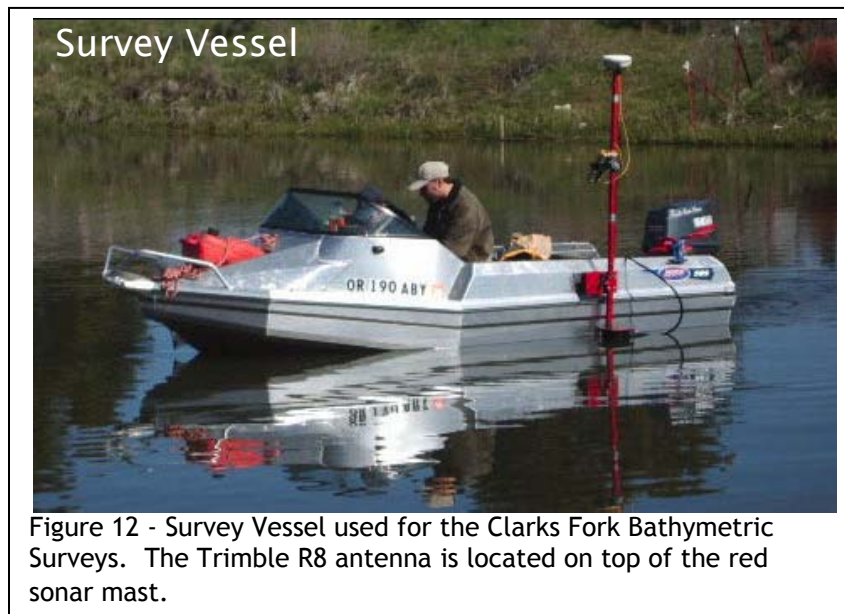


LiDAR Data Acquisition and Processing: Clarks Fork & Hot Springs Creek, Montana

Prepared by Watershed Sciences, Inc.

## 6.2 Bathymetric Survey - Instrumentation and Methods

Bathymetric data were collected using a Biosonics DT-X digital echo-sounder coupled with a single beam 200 kHz 6 degree digital transducer. Bathymetric data were collected at a frequency of 5 Hz (0.2 seconds). Backup positioning and time stamp information was provided by a Trimble AG-132 GPS with the signal being routed into the Biosonics echosounder and coupled in real-time with the hydroacoustic data. The AG-132 also provided navigation information which was fed into an onboard computer



and overlaid onto pre-mapped transects. The survey vessel was a 14 foot Stabicraft powered by a 50 hp jet pump (Figure 20). The transducer was mounted to the side of the vessel and the face was submerged to a depth of approximately 21 cm.

In order to obtain accurate vertical positions, a Trimble R8 GPS antenna was mounted directly over the transducer and configured to record fast static data at a 1-Hz interval. During the hydroacoustic survey a Trimble R-7 was set up over same survey monuments (certified by WGM Group) used during the LiDAR survey (Table 1). The fast-static data were then corrected during post-processing in the same method as the airborne GPS. (Section 3.2)

## 6.3 Bathymetric Data Processing

Bathymetric data were processed using Visual Analyzer 4.1 with depth measurements being reported every 0.2 seconds. Automated algorithms for bottom detection were used as a best “first guess” of the bottom location. All data files were extensively examined and edited by hand in cases where the computer algorithm failed to detect the correct location of the bottom. The SONAR data was then joined with the post processed GPS files based on the time stamp. A straight line interpolation was used to fill in the difference in data densities of the two data sets (5 Hz -SONAR, 1 Hz - GPS). A calibration data set was collected downstream of the Clarks Fork survey to check for any time offsets between the two data sets and it was determined that the best fit for the data was with a zero time offset.

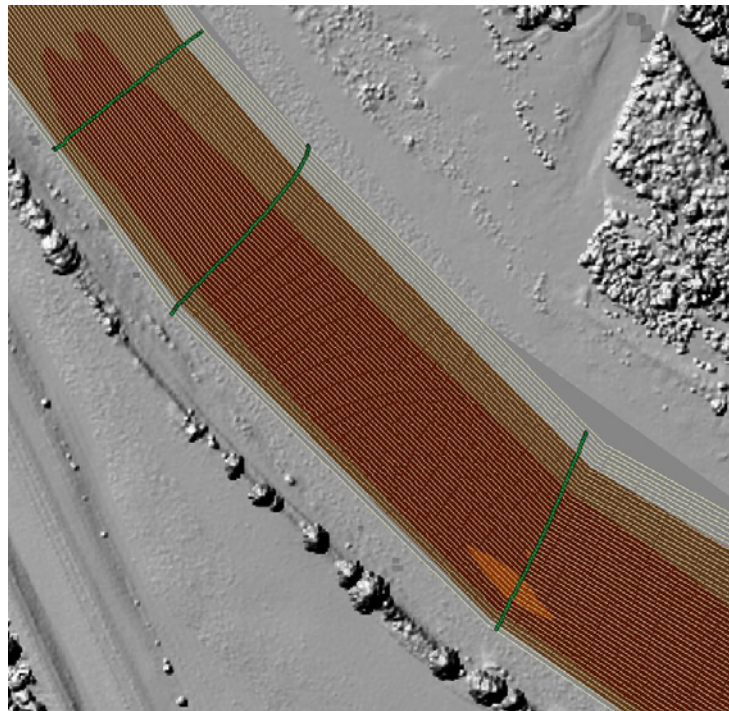
Vertical positions attained through post processed GPS exhibited a low degree of variability, but some additional processing was required to filter vertical positions that differed significantly from the standard deviation of all points collected. This variability was presumably due to dilution of position from lost satellites (especially near the river banks and

bridges) and/or degraded post processing solution (introduced from boat movement or undesirable satellite constellation).

Bathymetric elevations along each cross-section were derived by associating the hydroacoustic depth with the GPS position via GPS timestamp. Bottom surface positions and elevations were then calculated by subtracting the depth measurement from GPS position. Raw bathymetric positions were then spatially summarized in ArcGIS for development of an interpolated bathymetric surface model.

Firstly a surface was interpolated between cross sections forcing interpolation linearly based on relative position in the stream. This prevented direct interpolation between bank points and thalweg points or opposite bank points due to the positioning of the cross section in the stream (Fig 13).

*Figure 13.* 2-D image of linear interpolation between cross-sections overlaid on LiDAR-derived highest-hit hillshade of Clarks Fork Survey Site.



## 6.4 Bathymetric Accuracy Assessment

Unlike the LiDAR bare earth model, there is no easy way to directly survey the river bottom (at these depths) to statistically evaluate the accuracy of the bathymetric model. However, we would like to discuss the expected bathymetric accuracy in terms of component accuracies including: 1) positional accuracy of sonar/transducer; 2) timing differences between the GPS and sonar; 3) boat attitude at the time of sounding (i.e. pitch, roll, yaw); 4) instrumentation tolerances; and 5) interpolation error.

Positional accuracy of the sonar/transducer (#1) was discussed previously (Section 6.2 - 6.3) and after post-processing, is not considered a significant source of error. Timing difference between the GPS and sonar was measured using a calibration transect at the beginning of the survey. The boat attitude was not measured and therefore could not be quantified. However, the river surface conditions and boat configuration were relatively constant throughout the surveys and this error was considered relatively minor. The accuracy of the echosounder is +/- 5 cm, and the minimum sounding depth was 0.50 meters. The most significant source of potential error is interpolation, both between distant cross-sections and between the hydro acoustically derived bathymetric surface and the LiDAR derived bank elevations.

## 7. Combined Elevation Model

Integration of the hydroacoustic data with the LiDAR data was a five step process.

- 1) Create an interpolated bathymetry surface of the main channel using linear interpolation between main-channel transects.  
**Software:** ArcGIS 9.3.1
- 2) Warp interpolated main-channel surface to fit stream features (i.e. bends, islands, narrows).  
**Software:** ArcGIS 9.3.1
- 3) Generate regular points within main channel and assign elevations from warped interpolated bathymetry surface.  
**Software:** ArcGIS v.9.3.1
- 4) Extract ground model-key points from terrestrial LiDAR using digitized water and island masks.  
**Software:** MicroStation v.8, TerraScan v.9.001, ArcGIS v.9.3.1
- 5) Combine main-channel points, LiDAR ground returns, breakpoints, and back-channel depth points into a single elevation model.  
**Software:** Microstation v.8, ArcGIS v. 9.3.1
- 6) Manually inspect combined bathymetric mode for interpolation errors removing erroneous features when identified.  
**Software:** Microstation v.8, ArcGIS v. 9.3.1

## 7.1 Bathymetric Processing

It was necessary to generate the bathymetry model in multiple stages to prevent mis-interpolation between main-channel transects and back-channel or water edge points. First a TIN surface was interpolated from main-channel transects only. This forced the direction of interpolation to follow the river current. Because meander of the river was such that direct linear interpolation between cross-sections did not adequately capture the character of the river, the interpolated surface was warped to better fit the river banks. Additional points were then generated between transects and assigned elevation based on the interpolated main-channel surface. These newly generated points were used to represent the main channel in the final model (Figure 14). Because the new points are more evenly distributed throughout the main channel they create a more accurate bathymetric representation when combined with ground points at the water edge.

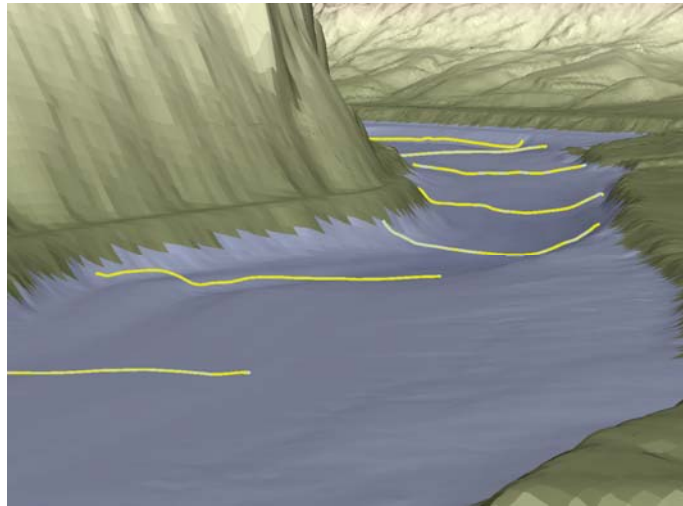


Figure 14 - Hydroacoustic cross sections displayed over the combined LiDAR and bathymetric models for the Clark Fork Study Site (vertical exaggeration = 2.0)

## 7.2 Terrestrial LiDAR Extraction

Extracting the terrestrial LiDAR data required a water mask digitized using LiDAR intensity images and ground models. Ground classified LiDAR points within the water mask were reclassified to an intermediate class so the bathymetry points could be used to develop a seamless model. A classification routine was run in TerraScan (LiDAR point processing software) to generate a new ground surface from bathymetry points and LiDAR points. The parameters for this routine started with an initial points spacing of 5 m then added or removed ground points as necessary to represent the full density LiDAR ground model within a vertical tolerance of +/- 0.1m.

## 7.3 Combined Elevation Model

The final integrated model was developed by combining 1) main-channel bathymetry points from the surface interpolated between hydroacoustic cross-sections, 2) model key points extracted from the terrestrial LiDAR data, 3) back-channel bathymetry points directly from the hydro acoustic survey. In Microstation v.8, an integrated surface was interpolated from the combined points generating a seamless representation of both the terrestrial and aquatic bare-earth. (Figures 15, 16)

*Figure 15. 3D image derived from LiDAR and Bathymetric data looking southeast along Clarks Fork*

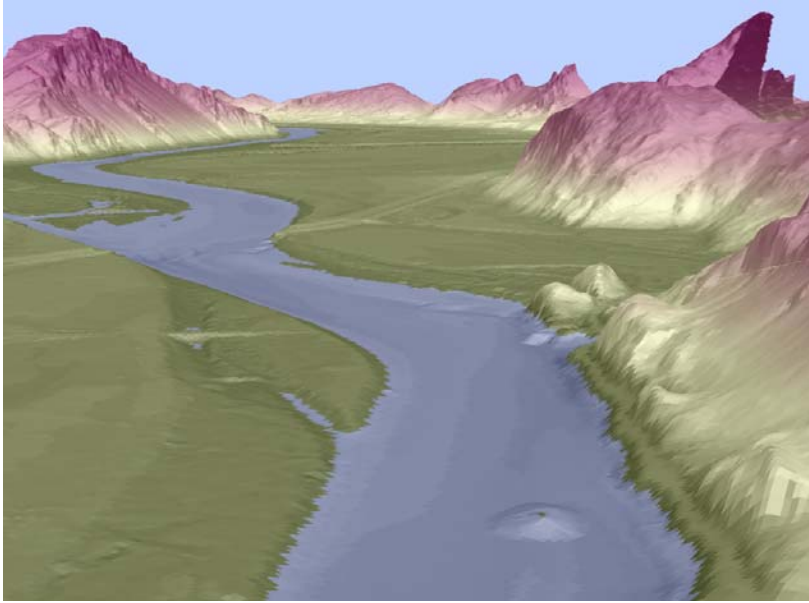
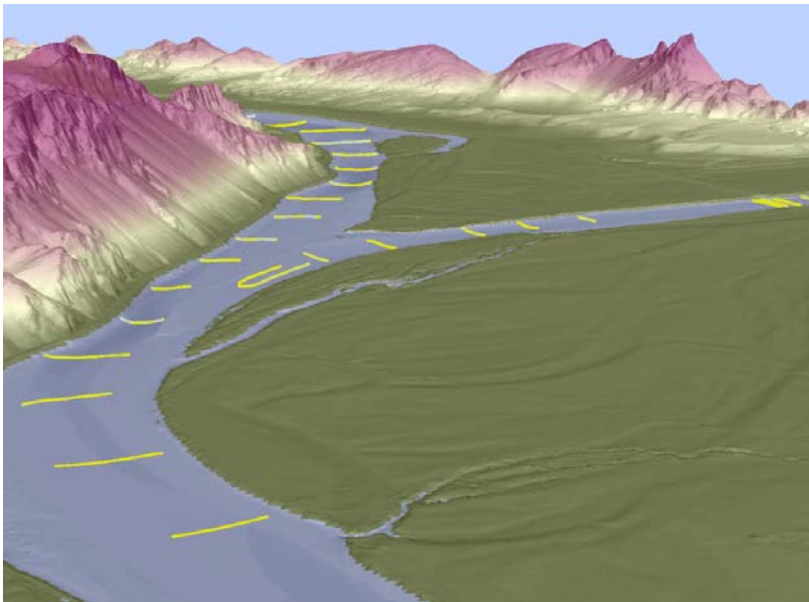


*Figure 16. 3D image derived from LiDAR and Bathymetric data overlaid with cross sections looking southeast along Clarks Fork*



## 8. Projection/Datum and Units

	<b>Projection:</b>	Montana State Plane FIPS 2500
<b>Datum</b>	<b>Vertical:</b>	NAVD88 Geoid03
	<b>Horizontal:</b>	NAD83
<b>Units</b>	<b>Vertical:</b>	U.S. Survey feet
	<b>Horizontal:</b>	International feet

## 9. Deliverables

<b>Point Data:</b>	<ul style="list-style-type: none"> <li>• All laser returns (LAS v. 1.2 format)</li> <li>• Ground returns (LAS v. 1.2 format)</li> <li>• Combined Elevation Model (ASCII text format)</li> </ul>
<b>Vector Data:</b>	<ul style="list-style-type: none"> <li>• Tile Index of LiDAR points (shapefile format)</li> <li>• 2 ft Contours (dxf format)</li> </ul>
<b>Raster Data:</b>	<ul style="list-style-type: none"> <li>• Elevation models (3-ft resolution) <ul style="list-style-type: none"> <li>• Bare Earth Model (ESRI GRID format)</li> <li>• Highest Hit Model (ESRI GRID format)</li> </ul> </li> <li>• Intensity images (GeoTIFF format, 1.5-ft resolution)</li> </ul>
<b>Data Report:</b>	Full report containing introduction, methodology, and accuracy

## 9. Selected Images

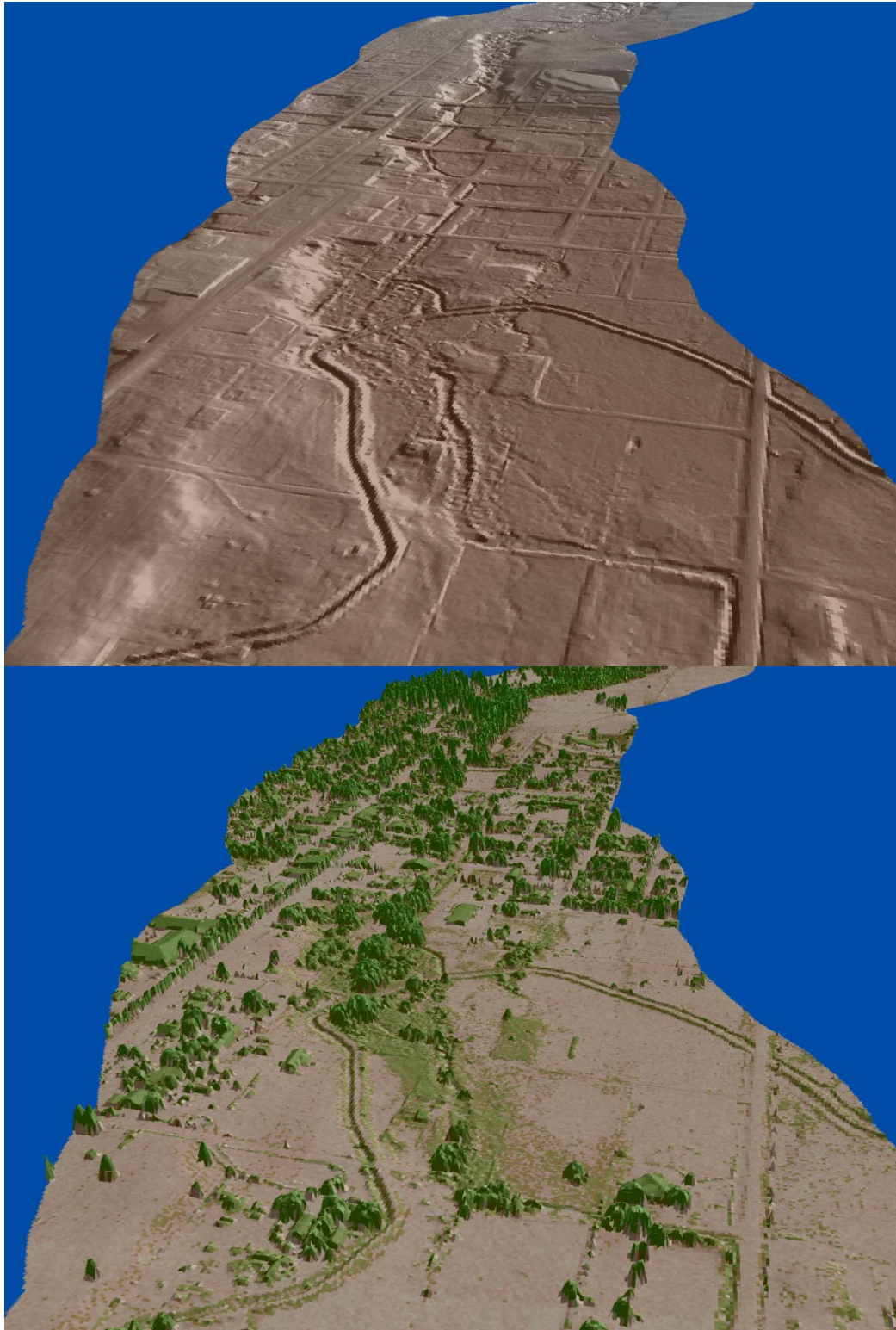
*Figure 17. 3D view looking North down Clarks Fork to its confluence with the Flathead River. The top image is derived from ground-classified LiDAR points and the bottom image is derived from the highest hit LiDAR points.*



LiDAR Data Acquisition and Processing: Clarks Fork & Hot Springs Creek, Montana

*Prepared by Watershed Sciences, Inc.*

*Figure 16. 3D view looking West over the town of Hot Springs, MT. The top image is derived from ground-classified LiDAR points and the bottom image is derived from the highest hit LiDAR points.*



**LiDAR Data Acquisition and Processing: Clarks Fork & Hot Springs Creek, Montana**

*Prepared by Watershed Sciences, Inc.*

Figure 17. 3D view looking South to the confluence of Flathead River and Clarks Fork. The top image is derived from ground-classified LiDAR points and the bottom image is derived from the highest hit LiDAR points.

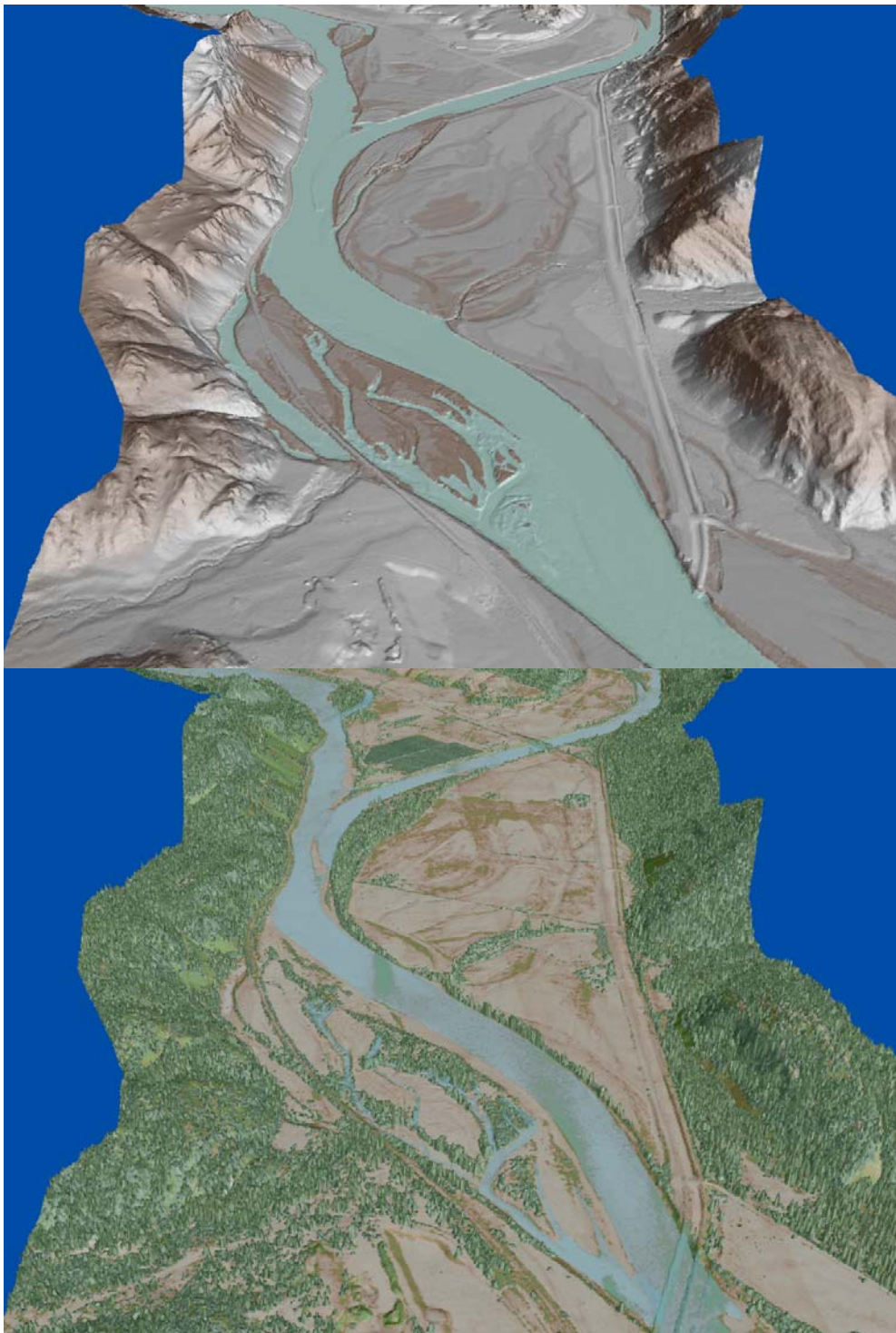


*Figure 18. Top image looking East and bottom image looking West across the town of Hot Springs, MT. Images are derived from LIDAR point cloud colored by height and textured by intensity.*

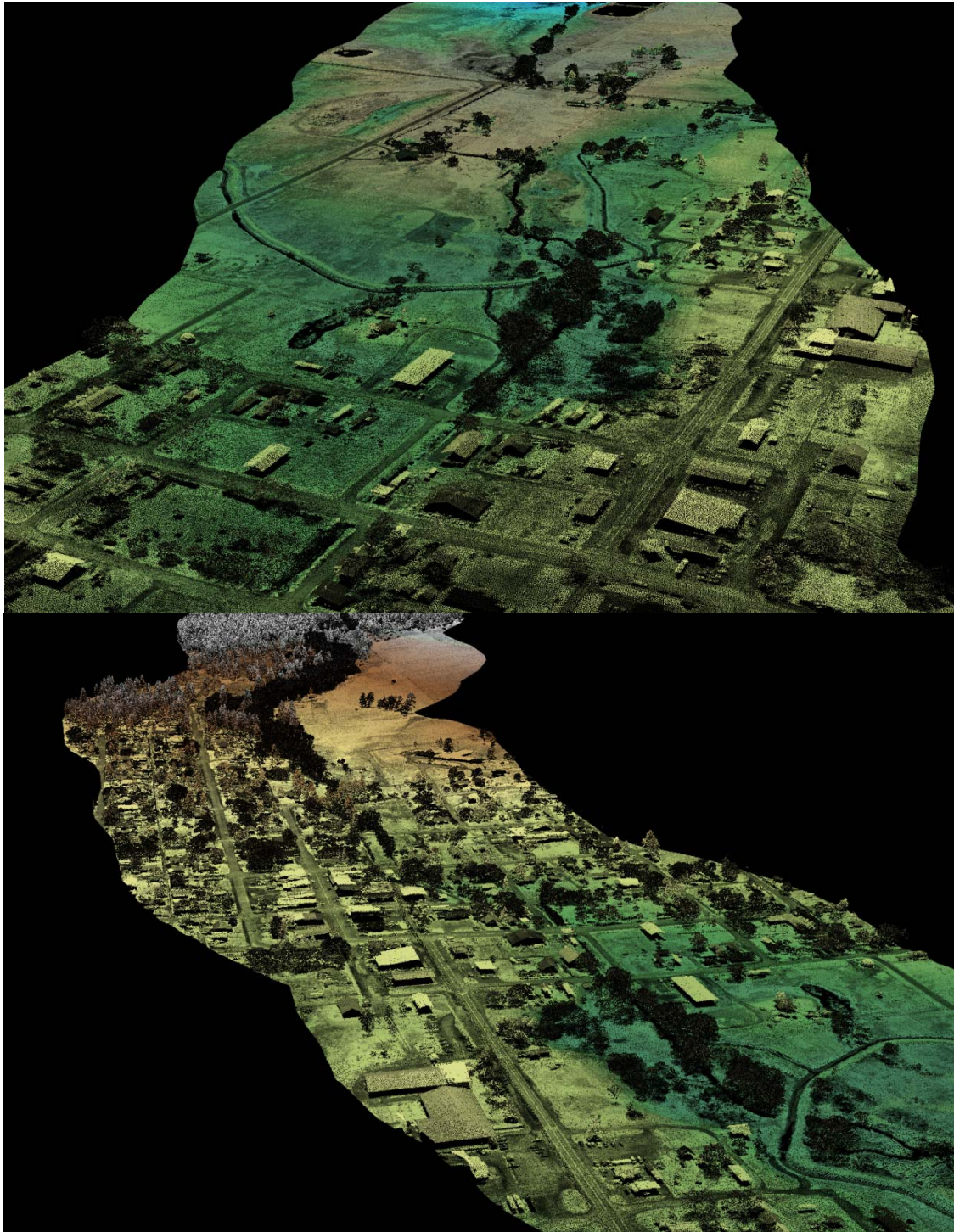
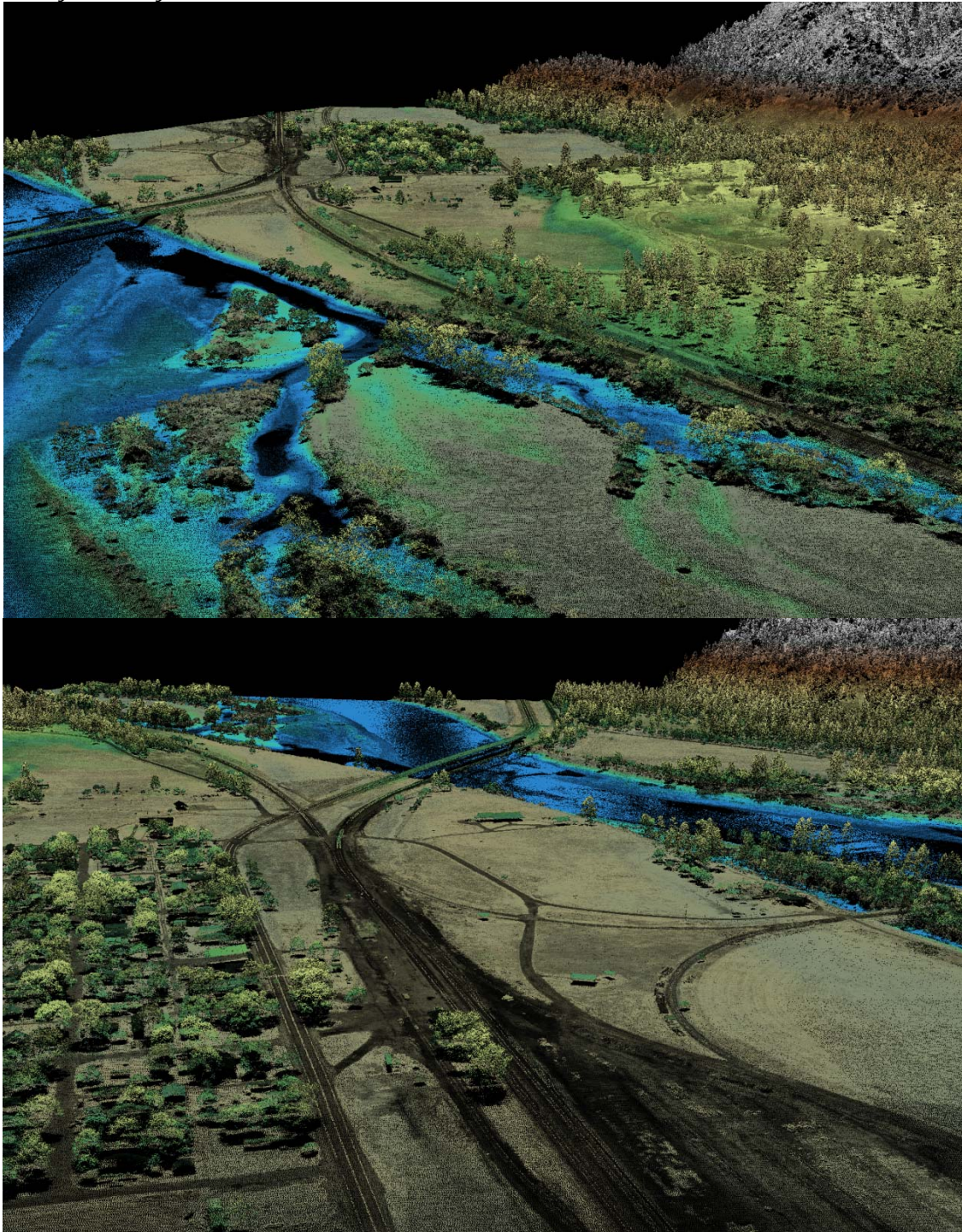


Figure 19. Top image looking Northwest and bottom image looking Southeast across the town of Paradise, MT on the Flathead River. Images are derived from LIDAR point cloud colored by height and textured by intensity.



## 10. Glossary

**1-sigma ( $\sigma$ ) Absolute Deviation:** Value for which the data are within one standard deviation (approximately 68<sup>th</sup> percentile) of a normally distributed data set.

**2-sigma ( $\sigma$ ) Absolute Deviation:** Value for which the data are within two standard deviations (approximately 95<sup>th</sup> percentile) of a normally distributed data set.

**Root Mean Square Error (RMSE):** A statistic used to approximate the difference between real-world points and the LiDAR points. It is calculated by squaring all the values, then taking the average of the squares and taking the square root of the average.

**Pulse Rate (PR):** The rate at which laser pulses are emitted from the sensor; typically measured as thousands of pulses per second (kHz).

**Pulse Returns:** For every laser pulse emitted, the Leica ALS 50 Phase II system can record *up to four* wave forms reflected back to the sensor. Portions of the wave form that return earliest are the highest element in multi-tiered surfaces such as vegetation. Portions of the wave form that return last are the lowest element in multi-tiered surfaces.

**Accuracy:** The statistical comparison between known (surveyed) points and laser points. Typically measured as the standard deviation ( $\sigma$ ) and root mean square error (RMSE).

**Intensity Values:** The peak power ratio of the laser return to the emitted laser. It is a function of surface reflectivity.

**Data Density:** A common measure of LiDAR resolution, measured as points per square meter.

**Spot Spacing:** Also a measure of LiDAR resolution, measured as the average distance between laser points.

**Nadir:** A single point or locus of points on the surface of the earth directly below a sensor as it progresses along its flight line.

**Scan Angle:** The angle from nadir to the edge of the scan, measured in degrees. Laser point accuracy typically decreases as scan angles increase.

**Overlap:** The area shared between flight lines, typically measured in percents; 100% overlap is essential to ensure complete coverage and reduce laser shadows.

**DTM / DEM:** These often-interchanged terms refer to models made from laser points. The digital elevation model (DEM) refers to all surfaces, including bare ground and vegetation, while the digital terrain model (DTM) refers only to those points classified as ground.

**Real-Time Kinematic (RTK) Survey:** GPS surveying is conducted with a GPS base station deployed over a known monument with a radio connection to a GPS rover. Both the base station and rover receive differential GPS data and the baseline correction is solved between the two. This type of ground survey is accurate to 1.5 cm or less.

## 11. Citations

Soininen, A. 2004. TerraScan User's Guide. TerraSolid.

## Appendix A

### LiDAR accuracy error sources and solutions:

Type of Error	Source	Post Processing Solution
GPS (Static/Kinematic)	Long Base Lines	None
	Poor Satellite Constellation	None
	Poor Antenna Visibility	Reduce Visibility Mask
Relative Accuracy	Poor System Calibration	Recalibrate IMU and sensor offsets/settings
	Inaccurate System	None
Laser Noise	Poor Laser Timing	None
	Poor Laser Reception	None
	Poor Laser Power	None
	Irregular Laser Shape	None

### Operational measures taken to improve relative accuracy:

1. Low Flight Altitude: Terrain following is employed to maintain a constant above ground level (AGL). Laser horizontal errors are a function of flight altitude above ground (i.e., ~ 1/3000<sup>th</sup> AGL flight altitude).
2. Focus Laser Power at narrow beam footprint: A laser return must be received by the system above a power threshold to accurately record a measurement. The strength of the laser return is a function of laser emission power, laser footprint, flight altitude and the reflectivity of the target. While surface reflectivity cannot be controlled, laser power can be increased and low flight altitudes can be maintained.
3. Reduced Scan Angle: Edge-of-scan data can become inaccurate. The scan angle was reduced to a maximum of  $\pm 15^\circ$  from nadir, creating a narrow swath width and greatly reducing laser shadows from trees and buildings.
4. Quality GPS: Flights took place during optimal GPS conditions (e.g., 6 or more satellites and PDOP [Position Dilution of Precision] less than 3.0). Before each flight, the PDOP was determined for the survey day. During all flight times, a dual frequency DGPS base station recording at 1-second epochs was utilized and a maximum baseline length between the aircraft and the control points was less than 19 km (11.5 miles) at all times.
5. Ground Survey: Ground survey point accuracy (i.e. <1.5 cm RMSE) occurs during optimal PDOP ranges and targets a minimal baseline distance of 4 miles between GPS rover and base. Robust statistics are, in part, a function of sample size (n) and distribution. Ground survey RTK points are distributed to the extent possible throughout multiple flight lines and across the survey area.
6. 50% Side-Lap (100% Overlap): Overlapping areas are optimized for relative accuracy testing. Laser shadowing is minimized to help increase target acquisition from multiple scan angles. Ideally, with a 50% side-lap, the most nadir portion of one flight line coincides with the edge (least nadir) portion of overlapping flight lines. A minimum of 50% side-lap with terrain-followed acquisition prevents data gaps.
7. Opposing Flight Lines: All overlapping flight lines are opposing. Pitch, roll and heading errors are amplified by a factor of two relative to the adjacent flight line(s), making misalignments easier to detect and resolve.